IEEE Access
Multidisciplinary | Rapid Review | Open Access Journal

Received January 19, 2020, accepted February 4, 2020, date of publication February 12, 2020, date of current version February 24, 2020.

Digital Object Identifier 10.1109/ACCESS.2020.2973469

Discontinuous Dynamic Analysis of a Modified Duffing-Rayleigh System With a Piecewise Quadratic Function

WEN ZHANG[1], FUHONG MIN[1,2], JIAYUN CHEN[1], AND YIPING DOU[1]
[1]School of Electrical and Automation Engineering, Nanjing Normal University, Nanjing 210023, China
[2]Jiangsu Key Laboratory of New Power Batteries, Nanjing Normal University, Nanjing 210023, China

Corresponding author: Fuhong Min (minfuhong@njnu.edu.cn)

This work was supported in part by the National Natural Science Foundation of China under Grant 61971228, Grant 61871230, and Grant 21875112, in part by the Natural Science Foundations of Jiangsu Higher Education Institutions of China under Grant 19KJB520042, and in part by the Postgraduate Research and Practice Innovation Program of Jiangsu of China under Grant SJCX19_0199.

ABSTRACT The discontinuous dynamical behavior of a modified Duffing-Rayleigh system with a piecewise quadratic function is studied. The necessary and sufficient conditions for motion switchability at the velocity boundary are investigated through the theory of discontinuous dynamical systems. Various motions through the boundary are demonstrated by the parameter maps and coexisting bifurcation diagrams. The coexistence of an example system under different initial conditions is illustrated by attraction basins, and the trajectories in phase plane. The periodic and chaotic motions with different mapping structures are analyzed for a better understanding of the motion switching mechanism. Through Multisim, the circuit experiment proves the effectiveness of the theoretical analysis.

INDEX TERMS Duffing-Rayleigh oscillator, switching boundary, multistability, coexisting attractors.

I. INTRODUCTION

The Duffing oscillator is a typical nonautonomous system, which has been modeled in various fields of physics, mechanics and engineering. It can exhibit different periodic motions and chaotic phenomena due to the periodically excitation [1]–[4]. For instance, the strange attractors of Duffing oscillator with negative linear stiffness and damping were discussed through Poincaré map and the positive maximal Lyapunov exponent [5]. Chaotic attractors of the Duffing parametric equation under the quasi-periodic perturbation through the Melnikov method were studied via the homoclinic or heteroclinic bifurcation surfaces and phase portraits [6]. The study on the property of the dynamical Duffing system has been well served to the applications in engineering. The new method for state identification of the Duffing oscillator based on extreme learning machine was proposed to solve the problem in heavy computation cost and slow convergence rate [7]. The motion of the Duffing oscillator in different input states was carried out to obtain better ways of detecting weak signals in the background of strong noise [8]. The damped Duffing oscillator was investigated and used in the impact load identification method with deep Recurrent Neural Network [9]. Moreover, the combination of the Duffing system and other nonlinear systems have attracted increasing attention due to its rich dynamical behaviors, such as Van Der Pol-Duffing system [10], Rayleigh-Duffing system [11] and the memristive Duffing oscillator [12].

The Duffing-related oscillators in the above literatures belong to smooth dynamical systems, which can exhibit abundant nonlinear motions. However, non-smooth systems, more widespread than smooth systems in everyday life, can describe the actual systems more accurately. For example, the function in the Duffing-like system as the chaos generator was studied in detail and the bifurcation analysis was carried out to illustrate the underlying dynamics [13]. The Rayleigh-Duffing system, based on the generalized Rayleigh oscillator [14], was investigated through the fractal basin boundaries with varying the damping coefficient [15]. The chaotic dynamical behavior of fractional Duffing-Rayleigh-like system with an absolute function was discussed through bifurcation diagrams and phase portraits [16]. The parameter regions of the modified Duffing-Rayleigh system with an absolute function under the periodically driven were studied

The associate editor coordinating the review of this manuscript and approving it for publication was Di He.

This work is licensed under a Creative Commons Attribution 4.0 License. For more information, see http://creativecommons.org/licenses/by/4.0/

through the Melnikov function method [17]. In the non-smooth systems mentioned above, the dynamics of such nonlinear systems were often analyzed via Melnikov function method [18], which provides the necessary conditions for chaotic motions. However, such studies as the switching motions of the non-smooth systems have been rarely reported. The switching theory of flow focusing on the motion through the boundary was first proposed to present the necessary and sufficient conditions of the general discontinuous boundary, which has been gradually accepted and improved in recent years [19], [20]. For example, Luo and Gegg discussed the conditions of stick and non-stick motions for an oscillator controlled with periodic forcing, and they presented the analysis of the eigenvalue and periodic motions [21]. Luo and Thapa investigated the onset and vanishing of periodic motions on the discontinuity in a simplified brake system with a periodical excitation [22]. Luo and Huang analyzed the conditions for switching, grazing and sliding on the boundary and investigated the periodic and chaotic motion in the friction-induced, periodically-forced oscillator [23]. Luo and Connor discussed the dynamical behaviors of a gear transmission system with possible stick between two gears, and presented the chaotic and periodic responses with numerical simulation [24]. Min and Luo discussed the parameter characteristics for the partial and full chaotic synchronizations of two nonlinear gyroscope systems [25]. Min and Luo investigated the complex mechanism of projective synchronization of Chua circuits through the theory of discontinuous systems [26]. Chen and Min studied the switching motions on the displacement boundary in the periodically forced Duffing system with absolute function [27].

Motivated by the above literature survey, in this paper, a modified Duffing-Rayleigh system with a piecewise quadratic function is studied via the theory of discontinuous dynamical systems. The analytical conditions for periodic and chaotic motions at the velocity boundary are investigated for a better understanding of the mechanism of switching motion. The coexisting bifurcation diagrams and its corresponding phase planes are depicted to illustrate the system dynamical behaviors. The parameter maps and attractor basins are employed to explain the extreme sensitivity of such a nonlinear system. With the basic mappings defined, the periodic and chaotic responses of the system are presented through numerical simulation. The effectiveness of the analyzed model is validated by the circuit experimental results.

II. PROBLEM STATEMENT

In this section, the modified Duffing-Rayleigh system with a piecewise quadratic function is investigated. Due to the discontinuous nonlinearity, the phase plane of this system consists of two domains and a velocity boundary. The passable or grazing conditions of such a system on the boundary are analyzed and the switching sets are presented.

A. DESCRIPTION OF THE SYSTEM

The nonlinear modified Duffing-Rayleigh system with periodically forcing and a piecewise quadratic function was proposed by Zhang and Li [17]. The system has a broader region of chaotic attractor and parameter spaces than the ordinary Duffing-Rayleigh systems. The governing equation of such a system is given by

$$\ddot{x} - ax + bx^3 = \varepsilon[\mu(1 - |\dot{x}|)\dot{x} + f\cos\omega t] \tag{1}$$

or

$$\begin{cases} \dot{x} = y \\ \dot{y} = ax - bx^3 + \varepsilon[\mu(1 - |y|)y + f\cos\omega t] \end{cases} \tag{2}$$

where a, b are linear and nonlinear restoring parameters, f and ω amplitude and frequency of the external force, μ is the nonlinear damping coefficient,ε a small nonnegative constant. The system described by (1) or (2) is a non-smooth system and the total forces at the switching boundary are discontinuous.

In the phase plane, the state variable vector and the vector field are given by

$$\mathbf{x} \triangleq (x, \dot{x}) \equiv (x, y)^T \text{ and } \mathbf{F} \triangleq (y, F)^T \tag{3}$$

where $\mathbf{F}$ represents the scalar force.

Two domains and the switching boundary are described as

$$\begin{aligned} \Omega_1 &= \{(x, y)|y \in (V, \infty)\} \\ \Omega_2 &= \{(x, y)|y \in (-\infty, V)\} \end{aligned} \tag{4}$$

and

$$\partial\Omega_{\alpha\beta} = \left\{(x, y)|\varphi_{\alpha\beta}(x, y) \equiv y - V = 0\right\} \tag{5}$$

It should be emphasized that $\Omega_{\alpha\beta}$ stands for the boundary between two connectable domains Ω_α and Ω_β ($\alpha, \beta \in \{1, 2\}$ and $\alpha \neq \beta$) and V is a constant. The motion in each domain can be described as a discontinuous switching flow between the boundary in continuous dynamic systems as shown in Fig.1, where $V = 0$, the light gray and dark gray represent, respectively, the two different domains Ω_1 and Ω_2, and the dashed line stands for the velocity boundary.

From Luo [20], the dynamical system is described as

$$\dot{\mathbf{x}} = \mathbf{F}_\lambda^{(\kappa)}(\mathbf{x}, t), \quad (\kappa, \lambda \in \{0, 1, 2\}) \tag{6}$$

where the superscript κ and subscript λ with non-zero values represent two connectable domains for $\alpha, \beta \in \{1, 2\}$, which means that

$$\left.\begin{array}{l} \mathbf{F}_\alpha^{(\alpha)}(\mathbf{x}, t) = (y, F_\alpha(\mathbf{x}, t))^T \text{ in } \Omega_\alpha(\alpha \in \{1, 2\}) \\ \mathbf{F}_\alpha^{(\beta)}(\mathbf{x}, t) = (y, F_\beta(\mathbf{x}, t))^T \text{ in } \Omega_\alpha(\alpha \neq \beta \in \{1, 2\}); \\ \mathbf{F}_0^{(0)}(\mathbf{x}, t) = (V, 0)^T \text{ on } \partial\Omega_{\alpha\beta} \text{ for stick}, \\ \mathbf{F}_0^{(0)}(\mathbf{x}, t) \in [\mathbf{F}_\alpha^{(\alpha)}(\mathbf{x}, t), \mathbf{F}_\beta^{(\beta)}(\mathbf{x}, t)] \text{ on } \partial\Omega_{\alpha\beta} \\ \qquad\qquad \text{for non-stick} \end{array}\right\} \tag{7}$$

$$\mathbf{F}_\alpha(\mathbf{x}, t) = a^{(\alpha)}x - b^{(\alpha)}x^3 + \varepsilon\mu y - \varepsilon\mu y|y| + \varepsilon f\cos\omega t \tag{8}$$

$\mathbf{F}_\alpha^{(\alpha)}(\mathbf{x}, t)$ is the real vector field in the α-domain, $\mathbf{F}_\alpha^{(\beta)}(\mathbf{x}, t)$, controlled by the vector field in the β-domain, is the fictitious vector field in the α-domain. $\mathbf{F}_0^{(0)}(\mathbf{x}, t)$ is the vector field on the boundary, and it can induce the discontinuity of the vector for the whole system. The scalar force in the α-domain is

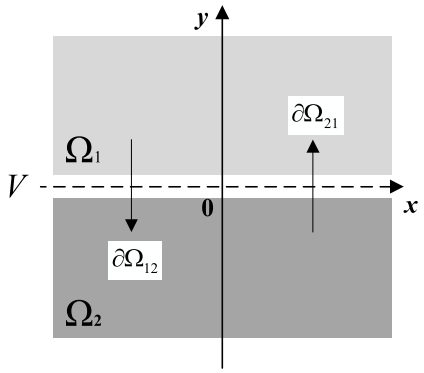

FIGURE 1. Domain partitions in phase plane.

$\mathbf{F}_\alpha(\mathbf{x}, t)$ and the forces in the two domains are expressed by (8), which includes the linear and nonlinear spring forces, the nonlinear damping force and the excitation force plus the friction force.

B. ANALYTICAL CONDITIONS

According to the theory of flow switchability [20], the necessary and sufficient conditions of the flow passing the boundary $\partial\Omega_{\alpha\beta}$ with $\mathbf{n}_{\partial\Omega_{\alpha\beta}} \to \Omega_\alpha$ can be expressed as

$$\left.\begin{aligned} &G^{(0,\alpha)}(\mathbf{x}_m, t_{m-}) = \mathbf{n}^T_{\partial\Omega_{\alpha\beta}} \cdot \mathbf{F}^{(\alpha)}(\mathbf{x}_m, t_{m-}) < 0, \\ &G^{(0,\beta)}(\mathbf{x}_m, t_{m+}) = \mathbf{n}^T_{\partial\Omega_{\alpha\beta}} \cdot \mathbf{F}^{(\beta)}(\mathbf{x}_m, t_{m+}) < 0 \end{aligned}\right\} \text{from } \Omega_\alpha \to \Omega_\beta$$
$$\left.\begin{aligned} &G^{(0,\beta)}(\mathbf{x}_m, t_{m-}) = \mathbf{n}^T_{\partial\Omega_{\alpha\beta}} \cdot \mathbf{F}^{(\beta)}(\mathbf{x}_m, t_{m-}) > 0, \\ &G^{(0,\alpha)}(\mathbf{x}_m, t_{m+}) = \mathbf{n}^T_{\partial\Omega_{\alpha\beta}} \cdot \mathbf{F}^{(\alpha)}(\mathbf{x}_m, t_{m+}) > 0 \end{aligned}\right\} \text{from } \Omega_\beta \to \Omega_\alpha \tag{9}$$

for $\mathbf{n}_{\partial\Omega_{\alpha\beta}} \to \Omega_\alpha$, where $\alpha, \beta \in \{1, 2\}$ and $\alpha \neq \beta$ with

$$\mathbf{n}_{\partial\Omega_{\alpha\beta}} = \nabla\varphi_{\alpha\beta} = (\partial_x\varphi_{\alpha\beta}, \partial_y\varphi_{\alpha\beta})^T_{(x_m, y_m)} \tag{10}$$

where $\nabla = (\partial_x, \partial_y)^T$ is the Hamilton operator with $\partial_x(\cdot) = \partial(\cdot)/\partial x$ and $\partial_y(\cdot) = \partial(\cdot)/\partial y$. The switching time t_m stands for the motion on the boundary and $t_{m\pm} = t_m \pm 0$ represents the motions in domains approaching the boundary, instead of on the boundary. The switching time t_{m+} and t_{m-} indicate the motion just approaching and leaving the boundary.

If the motion in the domain is tangent to the separation boundary $\partial\Omega_{\alpha\beta}$, the conditions for the grazing motion should be satisfied with

$$\left.\begin{aligned} &G^{(0,\alpha)}(\mathbf{x}_m, t_{m\pm}) = \mathbf{n}^T_{\partial\Omega_{\alpha\beta}} \cdot \mathbf{F}^{(\alpha)}(\mathbf{x}_m, t_{m\pm}) = 0, \\ &G^{(1,\alpha)}(\mathbf{x}_m, t_{m\pm}) = \mathbf{n}^T_{\partial\Omega_{\alpha\beta}} \cdot D\mathbf{F}^{(\alpha)}(\mathbf{x}_m, t_{m\pm}) > 0 \end{aligned}\right\} \text{in domain } \Omega_\alpha \tag{11}$$

for $\mathbf{n}_{\partial\Omega_{\alpha\beta}} \to \Omega_\alpha$ and

$$\left.\begin{aligned} &G^{(0,\beta)}(\mathbf{x}_m, t_{m\pm}) = \mathbf{n}^T_{\partial\Omega_{\alpha\beta}} \cdot \mathbf{F}^{(\beta)}(\mathbf{x}_m, t_{m\mp}) = 0, \\ &G^{(1,\beta)}(\mathbf{x}_m, t_{m\mp}) = \mathbf{n}^T_{\partial\Omega_{\alpha\beta}} \cdot D\mathbf{F}^{(\beta)}(\mathbf{x}_m, t_{m\mp}) < 0 \end{aligned}\right\} \text{in domain } \Omega_\beta \tag{12}$$

The necessary and sufficient conditions for the sliding motion on the boundary $\partial\Omega_{\alpha\beta}$ are given by

$$\left.\begin{aligned} &G^{(0,\alpha)}(\mathbf{x}_m, t_{m-}) = \mathbf{n}^T_{\partial\Omega_{\alpha\beta}} \cdot \mathbf{F}^{(\alpha)}(\mathbf{x}_m, t_{m-}) < 0 \\ &G^{(0,\beta)}(\mathbf{x}_m, t_{m+}) = \mathbf{n}^T_{\partial\Omega_{\alpha\beta}} \cdot \mathbf{F}^{(\beta)}(\mathbf{x}_m, t_{m+}) > 0 \end{aligned}\right\} \tag{13}$$

for $\mathbf{n}_{\partial\Omega_{\alpha\beta}} \to \Omega_\alpha$. It should be noted that the conditions are not valid on the boundary of system (1), and the relative motions are illustrated in [22], [23].

Using (5) and (10), the normal vector is defined as

$$\mathbf{n}_{\partial\Omega_{12}} = \mathbf{n}_{\partial\Omega_{21}} = (0, 1)^T \tag{14}$$

From (14), the normal vector of the velocity boundary tends to point to domain Ω_1. The zero and first G-function for $\alpha \in \{1, 2\}$ are

$$\left.\begin{aligned} &G^{(0,\alpha)}(\mathbf{x}_m, t_{m\pm}) = \mathbf{n}^T_{\partial\Omega_{\alpha\beta}} \cdot \mathbf{F}^{(\alpha)}(\mathbf{x}_m, t_{m\pm}) = \mathbf{F}_\alpha(\mathbf{x}_m, t_{m\pm}), \\ &G^{(1,\alpha)}(\mathbf{x}_m, t_{m\pm}) = \mathbf{n}^T_{\partial\Omega_{\alpha\beta}} \cdot D\mathbf{F}^{(\alpha)}(\mathbf{x}_m, t_{m\pm}) = D\mathbf{F}_\alpha(\mathbf{x}_m, t_{m\pm}) \\ &\quad = \nabla F_\alpha(\mathrm{x}, t) \cdot \mathbf{F}^{(\alpha)}(\mathbf{x}, t) + \partial_t F_\alpha(\mathbf{x}, t)|_{(\mathbf{x}_m, t_{m\pm})} \end{aligned}\right\} \tag{15}$$

and

$$\left.\begin{aligned} G^{(0,1)}(\mathbf{x}_m, t_{m\pm}) &= \mathbf{n}^T_{\partial\Omega_{12}} \cdot \mathbf{F}^{(1)}(\mathbf{x}_m, t_{m\mp}) = \mathbf{F}_1(\mathbf{x}_m, t_{m\mp}) \\ &= ax - bx^3 + \varepsilon\mu(1 - y)y + \varepsilon f\cos\omega t \\ G^{(0,2)}(\mathbf{x}_m, t_{m\pm}) &= \mathbf{n}^T_{\partial\Omega_{12}} \cdot \mathbf{F}^{(2)}(\mathbf{x}_m, t_{m\mp}) = \mathbf{F}_2(\mathbf{x}_m, t_{m\mp}) \\ &= ax - bx^3 + \varepsilon\mu(1 + y)y + \varepsilon f\cos\omega t \\ G^{(1,1)}(\mathbf{x}_m, t_{m\mp}) &= \mathbf{n}^T_{\partial\Omega_{12}} \cdot D\mathbf{F}^{(1)}(\mathbf{x}_m, t_{m\mp}) \\ &= D\mathbf{F}_1(\mathbf{x}_m, t_{m\mp}) \\ &= (a - 3bx^2)y + \varepsilon\mu(1 - 2y)\dot{y} - \varepsilon f\omega\sin\omega t \\ G^{(1,2)}(\mathbf{x}_m, t_{m\mp}) &= \mathbf{n}^T_{\partial\Omega_{12}} \cdot D\mathbf{F}^{(2)}(\mathbf{x}_m, t_{m\mp}) \\ &= D\mathbf{F}_2(\mathbf{x}_m, t_{m\mp}) \\ &= (a - 3bx^2)y + \varepsilon\mu(1 + 2y)\dot{y} - \varepsilon f\omega\sin\omega t \end{aligned}\right\} \tag{16}$$

From the equations above, the passable conditions of switching motions through the boundary can be written as

$$\left.\begin{aligned} &G^{(0,1)}(\mathbf{x}_m, t_{m-}) = \mathbf{F}_1(\mathbf{x}_m, t_{m-}) < 0, \\ &G^{(0,2)}(\mathbf{x}_m, t_{m+}) = \mathbf{F}_2(\mathbf{x}_m, t_{m+}) < 0 \end{aligned}\right\} \text{from } \Omega_1 \to \Omega_2 \tag{17}$$

$$\left.\begin{aligned} &G^{(0,1)}(\mathbf{x}_m, t_{m-}) = \mathbf{F}_1(\mathbf{x}_m, t_{m-}) > 0, \\ &G^{(0,2)}(\mathbf{x}_m, t_{m+}) = \mathbf{F}_2(\mathbf{x}_m, t_{m+}) > 0 \end{aligned}\right\} \text{from } \Omega_2 \to \Omega_1 \tag{18}$$

and the conditions of the grazing motion to the boundary can be expressed as

$$\left.\begin{aligned} &G^{(0,1)}(\mathbf{x}_m, t_{m\pm}) = \mathbf{F}_1(\mathbf{x}_m, t_{m-}) = 0 \\ &G^{(1,1)}(\mathbf{x}_m, t_{m\mp}) = D\mathbf{F}_1(\mathbf{x}_m, t_{m-}) > 0 \end{aligned}\right\} \text{in domain } \Omega_1 \tag{19}$$

$$\left.\begin{aligned} &G^{(0,2)}(\mathbf{x}_m, t_{m\pm}) = \mathbf{F}_2(\mathbf{x}_m, t_{m\mp}) = 0 \\ &G^{(1,2)}(\mathbf{x}_m, t_{m\mp}) = D\mathbf{F}_2(\mathbf{x}_m, t_{m\mp}) < 0 \end{aligned}\right\} \text{in domain } \Omega_2 \tag{20}$$

C. MAPPING STRUCTURES

The mapping structures for the periodic motion are illustrated by switching planes and generic mappings to describe the complex motions of the dynamical system. In phase plane, a trajectory in Ω_α which starts and ends at the switching boundary is portrayed in Fig.2. The mappings

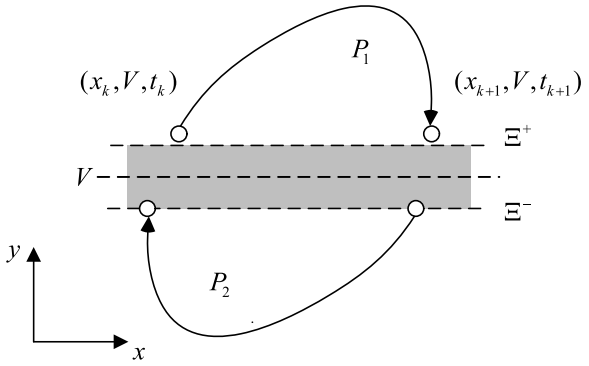

FIGURE 2. Switching planes and mappings.

P_α with the starting and ending points in Ω_α are, respectively, (x_k, V, t_k) and (x_{k+1}, V, t_{k+1}). Considering the velocity boundary, switching planes are defined as

$$\left.\begin{aligned}\Xi^+ &= \{(x_k, \omega t_k)|\dot{x}_k = V^+\}\\ \Xi^- &= \{(x_k, \omega t_k)|\dot{x}_k = V^-\}\end{aligned}\right\} \tag{21}$$

where $V^+ = \lim_{\delta\to 0}(V+\delta)$ and $V^- = \lim_{\delta\to 0}(V-\delta)$ with an arbitrary small $\delta > 0$.

Therefore, the two mappings are expressed as

$$P_1 : \Xi^+ \to \Xi^+, \quad P_2 : \Xi^- \to \Xi^- \tag{22}$$

From the relationships between switching planes and mappings, it can be concluded that

$$\left.\begin{aligned}P_1 &: (x_k, V^+, \omega t_k) \to (x_{k+1}, V^+, \omega t_{k+1})\\ P_2 &: (x_k, V^-, \omega t_k) \to (x_{k+1}, V^-, \omega t_{k+1})\end{aligned}\right\} \tag{23}$$

A generalized mapping structure for a periodic motion with non-stick can be written as

$$P = \underbrace{\left(P_2^{(k_{m2})} \circ P_1^{(k_{m1})}\right) \circ \ldots \circ \left(P_2^{(k_{12})} \circ P_1^{(k_{11})}\right)}_{m-terms} \tag{24}$$

where $k_{l\lambda} \in \{0, 1\}$, and $P_\lambda^{(0)} = 1$, $P_\lambda^{(k_{l\lambda})} = P_\lambda \circ P_\lambda^{(k_{l\lambda}-1)}$ ($l \in \{1, 2, \ldots, m\}$, $\lambda \in \{1, 2\}$).

From (24), the mapping structure of the simplest periodic motion can be defined as

$$P_{21} = P_2 \circ P_1 : \Xi^+ \to \Xi^- \tag{25}$$

Considering the equations above, the two mapping structures can be written as

$$\left.\begin{aligned}P_1 &: (x_k, V^+, t_k) \to (x_{k+1}, V^+, t_{k+1})\\ P_2 &: (x_{k+1}, V^-, t_{k+1}) \to (x_{k+2}, V^-, t_{k+2})\end{aligned}\right\} \tag{26}$$

Without sliding, the velocity boundary $V^+ = V^- = V$ occurs. During N-periods of excitation, for a periodic motion of $\mathbf{y}_{k+2} = P\mathbf{y}_k$ in $\mathbf{y}_k = (x_k, \omega t_k)^T$, the periodicity of the periodic motion is given by

$$x_{k+2} = x_k, \omega t_{k+2} = \omega t_k + 2N\pi \tag{27}$$

TABLE 1. Different color regions and the corresponding mapping structures.

Color	Mapping structure	color	Mapping structure
	P_{21}		$P_{(21)^5}$
	$P_{(21)^2}$		$P_{(21)^6}$
	$P_{(21)^3}$		$P_{(21)^7}$
	$P_{(21)^4}$		$P_{(21)^\infty}$

Therefore, the simplest periodic motions can be derived from (1) as,

$$\left.\begin{aligned}f_1^{(1)}(x_k, \omega t_k, x_{k+1}, \omega t_{k+1}) = 0\\ f_2^{(1)}(x_k, \omega t_k, x_{k+1}, \omega t_{k+1}) = 0\\ f_1^{(2)}(x_{k+1}, \omega t_{k+1}, x_{k+2}, \omega t_{k+2}) = 0\\ f_2^{(2)}(x_{k+1}, \omega t_{k+1}, x_{k+2}, \omega t_{k+2}) = 0\end{aligned}\right\} \tag{28}$$

The periodic motion for the generalized mappings can also be derived by the same method.

III. DISCONTINUOUS DYNAMICAL BEHAVIORS

In this section, from the passable and grazing conditions from (17) to (20), the parameter maps, global and local bifurcation diagrams and attraction basins will be presented, which can illustrate the coexistence and multistability of the modified Duffing-Rayleigh system. The coexisting periodic and chaotic motions are also depicted, based on the theory of flow switchability, through mapping structures and switching sections.

A. PARAMETER MAPS

The parameter maps can be used to visually illustrate the periodic and chaotic motions. Numerical simulations, using the conditions (17)-(20), are carried out through the symplectic scheme. The results, with the computational error tolerance 10^{-12}, and the initial conditions: $(t_0, x_0, y_0) = (0.0, 0.1, 0.1)$, $(0.0, -0.5, 0.5)$, are shown in Fig.3, where some discrete points represent the coexistence of different mapping structures, and the different color regions and their corresponding mapping structures are listed in Table 1. From Fig.3, it can be clearly observed how the changeable motions depend on the special regions of parameters.

B. BIFURCATION AND COEXISTENCE ATTRACTORS

For the study convenience, the modified Duffing-Rayleigh system is established with the parameters fixed as $a = 1$, $b = 1$, $\varepsilon = 0.1$, $\mu = 1.4$, $\omega = 1$. The bifurcation diagrams with varying f can be observed in Fig.4, where the orbits represent the increasing and decreasing f with the same initial conditions $(t_0, x_0, y_0) = (0.0, -0.5, 0.5)$, the acronyms 'PD', 'PF' and 'SN' stand for 'Period-Doubling Bifurcation', 'Pitchfork Bifurcation' and 'Saddle-Node Bifurcation'. It can be observed that the system exists complex dynamical behaviors with multistability. In Fig.4(a), the Duffing-Rayleigh

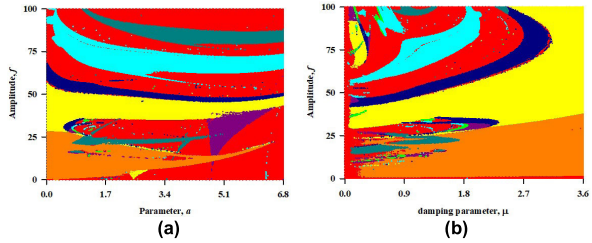

FIGURE 3. Parameter maps: (a) $a - f$ for $b = 1, \varepsilon = 0.1, \mu = 1.4, \omega = 1$; (b) $\mu - f$ for $a = 1, b = 1, \varepsilon = 0.1, \omega = 1$.

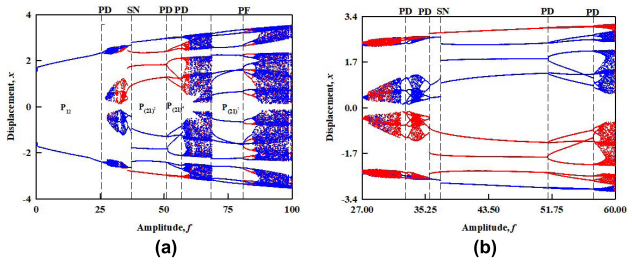

FIGURE 4. Bifurcation diagrams of switching displacement on the boundary with varying amplitude f: (a) $f \in [0, 100]$; (b) $f \in [27, 60]$.

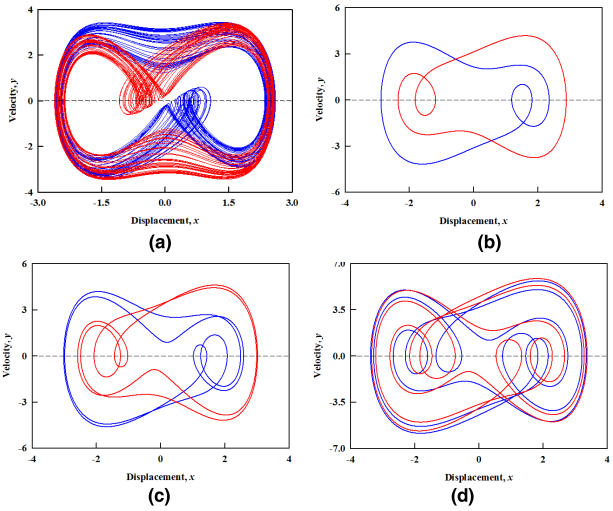

FIGURE 5. The coexistence phase planes with $a = 1, b = 1, \varepsilon = 0.1, \mu = 1.4, \omega = 1$ and: (a)$f = 31.6$, with $P_{(21)^\infty}$; (b)$f = 44$,with $P_{(21)^2}$ (c) $f = 54$,with $P_{(21)^4}$ (d)$f = 82.5$,with $P_{(21)^7}$.

TABLE 2. Coexistence mapping structures of the ranges of parameter f.

Coexisting mapping structures	Ranges of f	Coexisting mapping structures	Ranges of f
$P_{(21)^\infty}$ with $P_{(21)^\infty}$	(27.00,32.09)	$P_{(21)^4}$ with $P_{(21)^4}$	(34.81,35.82)
$P_{(21)^2}$ with $P_{(21)^2}$	(32.09,32.67)	$P_{(21)^2}$ with $P_{(21)^2}$	(35.82,51.22)
$P_{(21)^7}$ with $P_{(21)^7}$	(32.67,33.42)	$P_{(21)^4}$ with $P_{(21)^4}$	(51.22,57.16)
$P_{(21)^\infty}$ with $P_{(21)^\infty}$	(33.42,34.81)	$P_{(21)^\infty}$ with $P_{(21)^\infty}$	(57.16,60.00)

system is firstly changed from period-1 with P_{21} to chaos through period doubling bifurcation at $f = 25.6$, and then goes back to period-2 with $P_{(21)^2}$ through saddle node bifurcation at $f = 37.2$. After two period doubling bifurcation at $f = 60.0$ and $f = 56.9$, the system turns into chaotic motion through a series of period doubling bifurcation. Then, through a saddle node bifurcation at $f = 68.3$ and a pitchfork bifurcation at $f = 80.8$, the Duffing-Rayleigh system enters into chaotic motion again. To highlight the coexisting part of the bifurcation, the bifurcation of f is zoomed to $[27, 60]$ as shown in Fig.4(b), where the step is $\Delta f = 0.02$. In Fig.4(b), two chaotic motions exist simultaneously for $f \in [27.0, 32.1]$. From $f = 32.01$, it is the saddle node bifurcation that leads the system into period motion, then the system returns to chaotic motion again through period doubling bifurcation at $f = 32.7$. After reverse period doubling bifurcation at $f = 35.8$, the system goes into periodic motion.

The phase planes are depicted in Fig.5, where the coexisting period or chaotic behaviors are demonstrated, and it is relative to the coexisting bifurcation diagrams in Fig.4 (a) and (b). The coexisting trajectories with the blue and red cures are symmetric to the origin in phase planes, with the initial conditions $(t_0, x_0, y_0) = (0.0, 2.128, -1.691)$ and $(0.0, -0.018, 2.331)$ in Fig.5 (a), $(0.0, 1.727, 3.841)$ and $(0.0, 2.177, 3.841)$ in Fig.5 (b), $(0.0, 1.635, -1.701)$ and $(0.0, 2.925, 1.485)$ in Fig.5 (c), $(0.0, 3.019, -2.713)$ and $(0.0, 2.698, 5.032)$ in Fig.5 (d), respectively. The specific coexistence ranges of the amplitude parameter f are listed in Table 2.

Suppose $a = 1, b = 1, \varepsilon = 0.1, \omega = 1, f = 65$, the global bifurcation diagram of μ for $\mu \in [0, 3.6]$ with $\Delta\mu = 0.002$ is shown in Fig.6 (a), and the local bifurcation diagram for $\mu \in [1.8, 3.6]$ is shown in Fig.6 (b), where the coexistence distribution can be clearly observed. The system goes into chaos from periodic motion through a saddle node bifurcation at $\mu = 0.212$. The pitchfork bifurcation happens at $\mu = 0.723$, which shows that the routes of the damping parameter μ are complementary in terms of the dynamical properties. The saddle node bifurcation at $\mu = 1.165$ leads to the chaotic motion. Finally, the system motion becomes periodic through the reverse period doubling bifurcations for $\mu = 2.070$, $\mu = 2.544$.

Fix $b = 1, \varepsilon = 0.1, \mu = 1.4, \omega = 1, f = 65$ with varying parameter a, the periodic motion, chaos, as well as coexisting bifurcation modes can be observed as shown in Fig.7, where the bifurcation diagram is shown in Fig.7 (a) for $a \in [0, 4]$ with $\Delta a = 0.004$. Increasing a, the motion route is from a series of period-doubling to chaos, and then it diverges to the end. Decreasing a, the route to chaos is similar to that of increasing a. In Fig.7 (b), the coexisting bifurcation diagrams are for $a \in [0, 0.4]$ with $\Delta a = 0.0002$, where the mapping structures $P_{(21)^4}$ with $P_{(21)^4}$, $P_{(21)^7}$ with $P_{(21)^7}$ and $P_{(21)^\infty}$ with $P_{(21)^\infty}$ are also observed. From Fig.7 (b), the system gets into chaos through a series of period doubling bifurcations for $a = 0.13$, $a = 0.21$. The coexistence motions of this system and the corresponding ranges of a and μ are listed in Table 3.

To sum up, the modified Duffing-Rayleigh system is extremely sensitive to the change of parameter or initial condition, which means that the rich dynamical behavior can

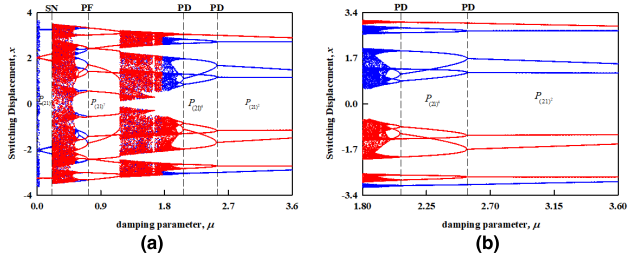

FIGURE 6. Bifurcation diagrams of switching displacement with μ: (a) $\mu \in [0, 3.6]$; (b) $\mu \in [1.8, 3.6]$.

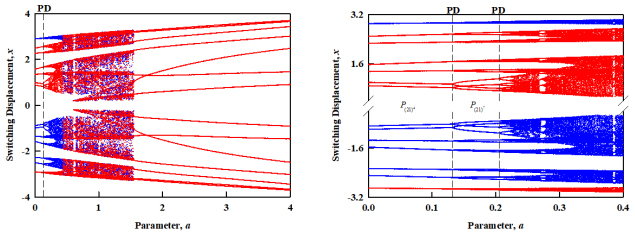

FIGURE 7. Bifurcation diagrams of switching displacement with a: (a)$a \in [0.0, 4.0]$; (b)$a \in [0.0, 0.4]$.

TABLE 3. Coexistence mapping structures of the ranges of parameter a and μ.

Coexisting mapping structures	Ranges of μ	Ranges of a
$P_{(21)^2}$ with $P_{(21)^2}$	(0.00,0.21) (2.54,3.60)	
$P_{(21)^4}$ with $P_{(21)^4}$	(2.07,2.54)	(0.00,0.13)
$P_{(21)^7}$ with $P_{(21)^7}$	(0.54,1.16) (1.99,2.07)	(0.13,0.21)
$P_{(21)^\infty}$ with $P_{(21)^\infty}$	(1.8,1.99)	(0.21,0.4)

be observed by varying parameter or initial condition. All of the bifurcation diagrams and phase planes can be homologized with various motion states of parameter mappings in Fig.3, which are determined by the conditions of grazing and passable flow, described in (17) - (20).

C. COEXISTENCE AND ATTRACTION BASINS

From the bifurcation diagrams above, it can be concluded that the system, with the same parameter sets but different initial conditions, may have multiple states. For the comprehensive observation of the coexistence of the special parameter value, attraction basins are used to illustrate the motions with distinct initial condition.

According to Fig.6 (a) and (b), the coexistence of the mapping structures $P_{(21)^2}$ with $P_{(21)^2}$ can be observed with $\mu = 3, a = 1, b = 1, \varepsilon = 0.1, \omega = 1, f = 65$ as shown in Fig. 8, where the corresponding attraction basins for left and right period-2 attractors are depicted in yellow and green, respectively, and the coexisting trajectories with the blue and red curves are presented with the initial conditions (0.0,2.625,−1.401) and (0.0,1.937,4.237) in Fig. 8(c). The coexistence of the mapping structures $P_{(21)^\infty}$ with $P_{(21)^\infty}$, with $a = 1, b = 1, \varepsilon = 0.1, \mu = 1.4, \omega = 1,$

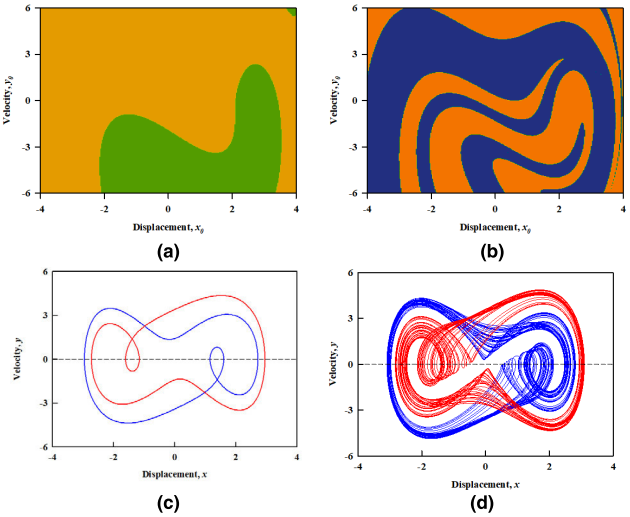

FIGURE 8. Attraction basins and corresponding phase planes : (a)attractors basin and (c) the coexisting periodic orbits with $a = 1, b = 1, \varepsilon = 0.1, \mu = 3, \omega = 1, f = 65$; (b) attractors basin and (d) the coexisting chaotic attractors with $a = 1, b = 1, \varepsilon = 0.1, \mu = 1.4, \omega = 1, f = 59.4$.

$f = 59.4$, can be seen in Fig.8 (b), where the basins of chaotic attractors depending on different initial values are portrayed, with the blue and orange regions representing two symmetry chaotic attractors. The corresponding phase plane with the blue and red curves is also depicted with the initial conditions (0.0,1.668,−1.686) and (0.0,2.065,4.748) in Fig.8 (d), where the switching flow of the system is passable to the velocity boundary.

D. SIMULATION RESULTS

For the better understanding of the coexistence of motion switchability at the velocity boundary, the periodic motions for the Duffing-Rayleigh system are presented as shown in Fig.9, where the horizontal dashed line $V = 0$ is the velocity boundary. From (16), the switching G-function $G^{(0,1)}$ is equal to $G^{(0,2)}$ at the switching points, marked by white and green circles, respectively representing P_2 switching to P_1 and P_1 to P_2, the gray circular symbol stands for the starting point.

From the attraction basins and trajectories in phase planes in Fig.8 (a) and (c), the coexistence of periodic orbits with the mapping structures in $P_{(21)^2}$ with $P_{(21)^2}$ are presented with the initial conditions (0.0,2.625,−1.401) and (0.0,1.937,4.237) in Fig.9 (a) and (b). Note that (16) is symmetric to the origin in phase planes with respect to the function $|\dot{x}|\,\dot{x}$. The coexistence time histories of velocity are depicted in Fig.9 (c) and (d). Fig.9 (e) and (f) illustrate the time histories of G-functions, verifying the flow switchability of this dynamical system. The G-function for the piecewise function is the real flow in the corresponding domains, which means that the discontinuous flow is switched once the motion switched. It can be seen from Fig.9 (c) and (e) that, for the flow switching from domain-2 to domain-1, the G-functions satisfy $G^{(0,1)} > 0$ and $G^{(0,2)} > 0$, and for the

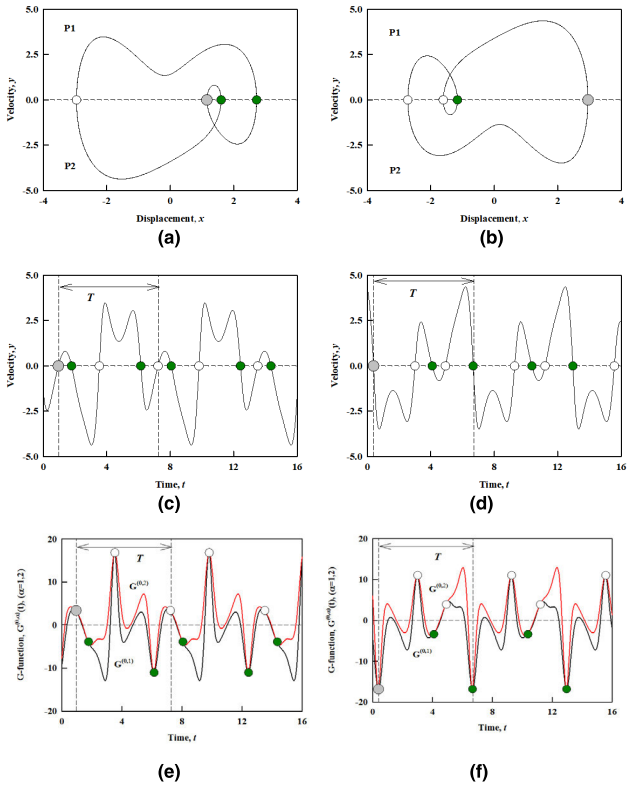

FIGURE 9. Coexisting periodic motions with the same mapping: (a)and(b)coexistent trajectories;(c)and(d)velocity time history;(e)and(f)G-function time history.

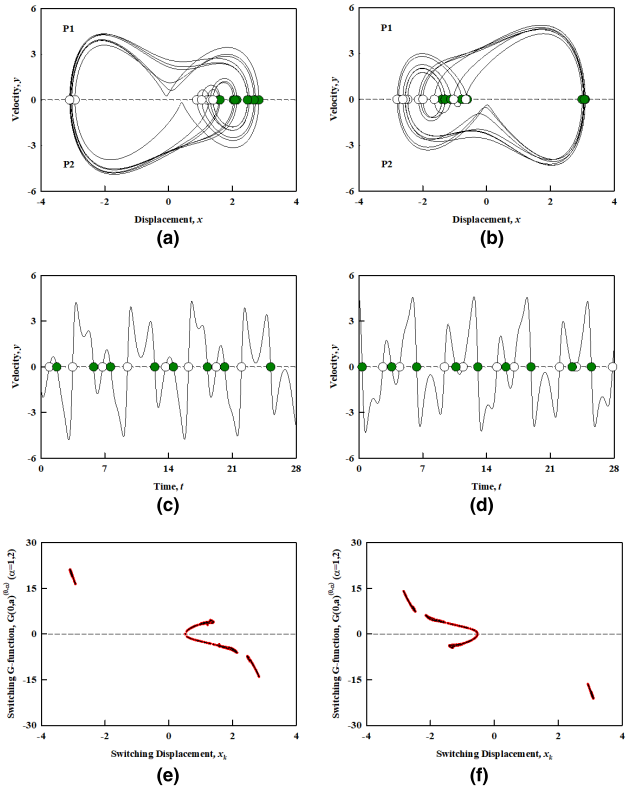

FIGURE 10. Coexisting chaotic motions with the mapping structures: (a) and (b) coexistent trajectories in phase plane; (c) and (d) velocity time history; (e) and (f) switching G-function distribution.

flow switching from domain-1 to domain-2, the G-functions satisfy $G^{(0,1)} < 0$ and $G^{(0,2)} < 0$. The behaviors like this are in consistent with (17) and (18). In one period, the G-function distribution along with periodical time in Fig.9 (e) and (f) are symmetrical to the origin, which are corresponding to the phase planes in Fig.9 (a) and (b).

The coexistence of chaotic attractors with the mapping structures in $P_{(21)^\infty}$ and $P_{(21)^\infty}$ is presented with the initial conditions (0.0,1.668,−1.686) and (0.0,2.065,4.748), as shown in Fig.10, the parameters of which are chosen as the same as Fig.8 (b) and (d). The partial trajectories in phase planes for the coexisting chaotic motion are illustrated in Fig.10 (a) and (b) and the time histories of velocity are presented in Fig.10 (c) and (d). The corresponding G-function distribution at the switching points versus the switching displacement are depicted in Fig.10 (e) and (f), where the force changes along the displacement are also illustrated. The switching points for $G^{(0,1)}$ and $G^{(0,2)}$ are represented by the black and red dots in Fig.10 (e) and (f). Therefore, for both the left and right sides of the switching displacement, the switching points of motion at the velocity boundary are passable because of the switching G-functions $G^{(0,1)} = G^{(0,2)} > 0$ for domain-1 and $G^{(0,1)} = G^{(0,2)} < 0$ for domain-2, which are also satisfied with the passable conditions given in (17) and (18), and the sliding motion doesn't exist for no switching points at the boundary.

IV. MULTISIM SIMULATION

The circuit model, using Multisim Simulation 14.0, is established for the Duffing-Rayleigh system with typical parameters as shown in Fig.11. From (2), the system circuit equations are given by

$$\begin{aligned} \frac{dx}{dt} &= \frac{1}{R_1 C_1} y \\ \frac{dy}{dt} &= -(\frac{R_{14}}{R_9} V_1 + \frac{R_{14}}{R_{10}}(-x) + \frac{R_{14}}{R_{11}} x^3 + \frac{R_{14}}{R_{12}}(-y) + \frac{R_{14}}{R_{13}} y\,|y|) \end{aligned} \tag{29}$$

The designed circuit in Fig.11 includes the integration of two state variables. The operational amplifiers OPAMP_3T_VIRTUAL, resistors and capacitors perform the basic operations of addition, integration and proportion. The nonlinear part in (2) is implemented by two multipliers AD633. The voltage supplies of active devices are of $\pm 12V$ and the gain of multiplier is set as $g = 1$. The absolute function is completed by the amplifier, resistors and one diode. Part of the circuit parameters are $R_1 = R_2 = 1M\Omega$, $C_1 = C_2 = 1\mu F$, $R_3 = R_4 = R_5 = R_6 = R_7 = R_8 = 10k\Omega$.

According to the inverting summing amplifier in (29), it can be deduced that

$$\begin{aligned} a &= R_{14}/R_{10}, b = R_{14}/R_{11}, \varepsilon = R_{14}/R_9 \\ \varepsilon\mu &= R_{14}/R_{12} = R_{14}/R_{13} \end{aligned} \tag{30}$$

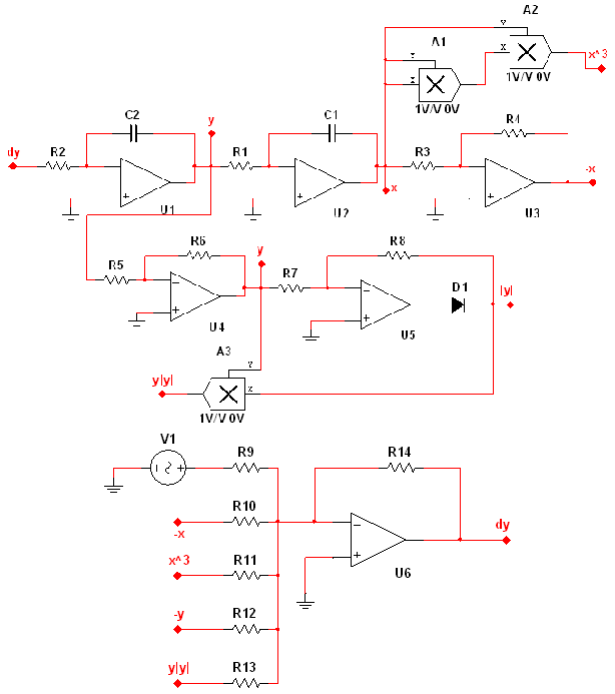

FIGURE 11. Circuit model for the modified Duffing-Rayleigh System.

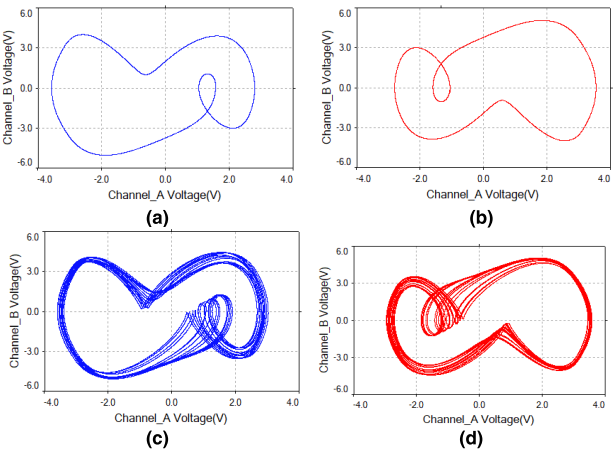

FIGURE 12. (a) and (b) Coexisting periodic orbits; (c)and(d) Coexisting chaotic trajectories.

Therefore, for the typical parameters $a = 1, b = 1, \varepsilon = 0.1, \mu = 3, \omega = 1, f = 65$, we get $R_{10} = R_{11} = R_{14} = 3k\Omega$, $R_{12} = R_{13} = 10k\Omega, R_9 = 30k\Omega$. The amplitude and frequency of V_1 are set to be 65V and 0.15915HZ respectively. The simulated phase portraits under different initial conditions are presented in Fig.12 (a) and (b). Similarly, we got Fig.12 (c) and (d) for $a = 1, b = 1, \varepsilon = 0.1, \mu = 1.4, \omega = 1, f = 59.4, R_{10} = R_{11} = R_{14} = 1.4k\Omega, R_{12} = R_{13} = 10k\Omega, R_9 = 14k\Omega$, with the amplitude 59.4V and frequency 0.15915Hz. Comparing curves in Fig.12 with that in Fig.8, it is obvious that the experiment results from Multisim are in good consistence with the numerical simulations, which verify the complicated dynamical phenomena of the modified Duffing-Rayleigh system.

V. CONCLUSION

In this paper, a periodically forced modified Duffing-Rayleigh system with a piecewise quadratic function is presented and discussed through the theory of switching flow, focusing on the switching behaviors on the boundary between two adjacent domains. The mapping structures of the system are investigated and analyzed. Through bifurcation diagrams and corresponding phase planes, the coexistence and multistability of such a system are demonstrated. The parameter maps and attraction basins illustrate that the dynamic behaviors of the example system are rich and affected greatly by both the parameter values and initial conditions. Chaotic and periodic motions are observed in the switching sections, which are conducive to a better understanding of the switching motion mechanism. The coexisting varying attractors are finally validated by Multisim software.

REFERENCES

[1] X. H. Li, Y. J. Shen, J. Q. Sun, and S. P. Yang, "New periodic-chaotic attractors in slow-fast Duffing system with periodic parametric excitation," *Sci. Rep.*, vol. 9, Aug. 2019, Art. no. 11185.
[2] Z. K. Peng and Z. Q. Lang, "Relationship between harmonic balance method and non-linear output frequency response function approach," *Proc. Inst. Mech. Eng. C, J. Mech. Eng. Sci.*, vol. 221, no. 12, pp. 1533–1543, Dec. 2007.
[3] I. Kirrou and M. Belhaq, "On the quasi-periodic response in the delayed forced Duffing oscillator," *Nonlinear Dyn.*, vol. 84, no. 4, pp. 2069–2078, Jun. 2016.
[4] Z. Hao, Q. Cao, and M. Wiercigroch, "Nonlinear dynamics of the quasi-zero-stiffness SD oscillator based upon the local and global bifurcation analyses," *Nonlinear Dyn.*, vol. 87, no. 2, pp. 987–1014, Jan. 2017.
[5] G. M. Mahmouda, A. Mohameda, and S. A. Alyb, "Strange attractors and chaos control in periodically forced complex Duffing's oscillators," *Phys. A, Stat. Mech. Appl.*, vol. 292, pp. 193–206, Mar. 2001.
[6] T. Jiang, Z. Yang, and Z. Jing, "Bifurcations and chaos in the duffing equation with parametric excitation and single external forcing," *Int. J. Bifurcation Chaos*, vol. 27, no. 08, Jul. 2017, Art. no. 1750125.
[7] G. Li, L. Zeng, L. Zhang, and Q. M. J. Wu, "State identification of duffing oscillator based on extreme learning machine," *IEEE Signal Process. Lett.*, vol. 25, no. 1, pp. 25–29, Jan. 2018.
[8] X. Liu and W. Ni, "Weak signal detection with duffing oscillator based on virtual instrument technology," *Int. J. Onl. Eng.*, vol. 11, no. 1, pp. 20–24, Jan. 2015.
[9] J. Zhou, L. Dong, W. Guan, and J. Yan, "Impact load identification of nonlinear structures using deep recurrent neural network," *Mech. Syst. Signal Process.*, vol. 133, Nov. 2019, Art. no. 106292.
[10] Z. Zhihong and Y. Shaopu, "Application of van der Pol–Duffing oscillator in weak signal detection," *Comput. Elect. Eng.*, vol. 41, pp. 1–8, Jan. 2015.
[11] H. B. Chen and L. Zou, "Global study of Rayleigh–Duffing oscillators," *J. Phys. A, Math. Theor.*, vol. 49, no. 16, 2016, Art. no. 165202.
[12] S. Sabarathinam, C. K. Volos, and K. Thamilmaran, "Implementation and study of the nonlinear dynamics of a memristor-based Duffing oscillator," *Nonlinear Dyn.*, vol. 87, no. 1, pp. 37–49, Jan. 2017.
[13] K. S. Tang, K. F. Man, G. Q. Zhong, and G. R. Chen, "Generating chaos with," *IEEE Trans. Circuits Syst. I, Reg. Papers Fundam. Theory*, vol. 48, no. 5, pp. 636–641.
[14] M. A. López and R. Martínez, "A note on the generalized Rayleigh equation: Limit cycles and stability," *J. Math. Chem.*, vol. 51, no. 4, pp. 1164–1169, Apr. 2013.
[15] M. Siewe Siewe, C. Tchawoua, and P. Woafo, "Melnikov chaos in a periodically driven Rayleigh–Duffing oscillator," *Mech. Res. Commun.*, vol. 37, no. 4, pp. 363–368, Jun. 2010.
[16] Y. L. Zhang and M. K. Luo, "Fractional Rayleigh–Duffing-like system and its synchronization," *Nonlinear Dyn.*, vol. 70, no. 2, pp. 1173–1183, Oct. 2012.
[17] Y. L. Zhang and C. Q. Li, "Fractional modified Duffing–Rayleigh system and its synchronization," *Nonlinear Dyn.*, vol. 88, no. 4, pp. 3023–3041, Jun. 2017.

[18] C. Cai, Z. Xu, and W. Xu, "Melnikov's analysis of time-delayed feedback control in chaotic dynamics," *IEEE Trans. Circuits Syst. I, Reg. Papers*, vol. 49, no. 12, pp. 1724–1728, Dec. 2002.
[19] A. C. J. Luo, "A theory for non-smooth dynamic systems on the connectable domains," *Commun. Nonlinear Sci. Numer. Simul.*, vol. 10, no. 1, pp. 1–55, Feb. 2005.
[20] D. Cheng, X. Hu, and T. Shen, "Discontinuous dynamical system," in *Analysis and Design of Nonlinear Control Systems*. Berlin, Germany: Springer-Verlag, 2012.
[21] A. C. J. Luo and B. C. Gegg, "Periodic motions in a periodically forced oscillator moving on an oscillating belt with dry friction," *J. Comput. Nonlinear Dyn.*, vol. 1, no. 3, pp. 212–220, Jul. 2006.
[22] A. C. J. Luo and S. Thapa, "Periodic motions in a simplified brake system with a periodic excitation," *Commun. Nonlinear Sci. Numer. Simul.*, vol. 14, no. 5, pp. 2389–2414, May 2009.
[23] A. C. J. Luo and J. Huang, "Discontinuous dynamics of a non-linear, self-excited, friction-induced, periodically forced oscillator," *Nonlinear Anal., Real World Appl.*, vol. 13, no. 1, pp. 241–257, Feb. 2012.
[24] F. Min and A. C. J. Luo, "On parameter characteristics of chaotic synchronization in two nonlinear gyroscope systems," *Nonlinear Dyn.*, vol. 69, no. 3, pp. 1203–1223, Aug. 2012.
[25] A. C. J. Luo and D. O'Connor, "Periodic and chaotic Motions in a Gear-pair transmission system with impacts," in *Nonlinear Science and Complexity*. Dordrecht, The Netherlands: Springer, 2011, pp. 13–24.
[26] F. Min and A. C. J. Luo, "Complex dynamics of projective synchronization of Chua circuits with different scrolls," *Int. J. Bifurcation Chaos*, vol. 25, no. 5, May 2015, Art. no. 1530016.
[27] J. Chen, F. Min, Q. Jin, and B. Ye, "Coexistence, bifurcation and chaos of a periodically forced duffing system with absolute nonlinearity," *Eur. Phys. J. Special Topics*, vol. 228, no. 6, pp. 1405–1419, Jul. 2019.

WEN ZHANG is currently pursuing the master's degree with the School of Electrical and Automation Engineering, Nanjing Normal University, China. Her current research interests include chaotic systems, memristive circuits, and dynamical analysis.

FUHONG MIN received the master's degree from the School of Communication and Control Engineering, Jiangnan University, in 2003, and the Ph.D. degree from the School of Automation, Nanjing University of Science and Technology, in 2007. From 2009 to 2010, she was a Postdoctoral Fellow with the School of Mechanical Engineering, Southern Illinois University. She is currently a Professor with the School of Electrical and Automation Engineering, Nanjing Normal University. Her research interests include memristive circuits, control and synchronization of chaotic circuits, and complex behavior of nonlinear power electronic circuits.

JIAYUN CHEN is currently pursuing the master's degree in electrical engineering with Nanjing Normal University, China. Her current research interest includes the analysis of nonlinear dynamical systems.

YIPING DOU received the master's and Ph.D. degrees from the Nanjing University of Aeronautics and Astronautics, in 1988 and 2002, respectively. From 2005 to 2006, he was a Visiting Scholar with the Faculty of Engineering, University of Technology Sydney, NSW, Australia. He is currently an Associate Professor with the School of Electrical and Automation Engineering, Nanjing Normal University. His research interests include the areas of system modeling and computation in engineering, nonlinear dynamics, electrical drives, and electrical machines.